ACS APPLIED MATERIALS & INTERFACES

Research Article

www.acsami.org

Nanocomposite of Polyaniline Nanorods Grown on Graphene Nanoribbons for Highly Capacitive Pseudocapacitors

Lei Li,[†] Abdul-Rahman O. Raji,[†] Huilong Fei,[†] Yang Yang,[‡] Errol L. G. Samuel,[†] and James M. Tour*[,†,‡,§]

[†]Department of Chemistry, [‡]Richard E. Smalley Institute for Nanoscale Science and Technology, [§]Department of Mechanical Engineering and Materials Science, Rice University, 6100 Main Street, Houston, Texas 77005, United States

Supporting Information

ABSTRACT: A facile and cost-effective approach to the fabrication of a nanocomposite material of polyaniline (PANI) and graphene nanoribbons (GNRs) has been developed. The morphology of the composite was characterized by scanning electron microscopy, transmission electron microscopy, X-ray photoelectron microscopy, and X-ray diffraction analysis. The resulting composite has a high specific capacitance of 340 F/g and stable cycling performance with 90% capacitance retention over 4200 cycles. The high performance of the composite results from the synergistic combination of electrically conductive GNRs and highly capacitive PANI. The method developed here is practical for large-scale development of pseudocapacitor electrodes for energy storage.

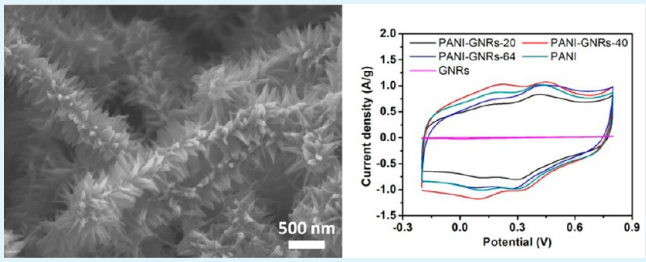

KEYWORDS: *polyaniline, graphene nanoribbons, supercapacitor, energy storage*

1. INTRODUCTION

Electrochemical capacitors are attracting interest due to their high power density, long life cycle, and well-known operational principles.[1−3] On the basis of their energy storage mechanism,[4] electrochemical capacitors can be categorized as electrical double layer capacitors (EDLCs) or pseudocapacitors. In an EDLC device, the electrostatic charge accumulation occurs at the interface between the electrode and the electrolyte. The performance of EDLCs is strongly dependent on the properties of the electrode and the electrolyte. EDLCs can provide ultrahigh power and excellent life cycles because of the nondegradative processes between the electrode and the electrolyte. The performance of EDLCs is determined by the available surface area of the electrodes and the finite charge separation between the electrode materials and the electrolyte.[1,5] However, in a pseudocapacitor (or redox supercapacitor), the fast and reversible faradic reaction near the surface determines its energy storage capability.[1,6] Typically, the specific capacitance of a pseudocapacitor electrode far exceeds that of an electrode operating as an EDLC.[7] Therefore, pseudocapacitors are preferred in applications where high capacitance is required.

Conducting polymers have been studied for their potential application as electrodes in energy storage devices.[8−11] Among conducting polymer, polyaniline (PANI) has attracted interest due to its high specific capacitance, good environmental stability, electroactivity, and doping−dedoping chemistry.[12−15] The major drawback that hinders the application of PANI in energy storage is its poor cyclic stability due to mechanical degradation by the large volumetric change in the doping/dedoping process; it is not stable to cycling through charge−discharge processes over long periods of time.[1] Interfacing other carbon materials with PANI is one effective way to improve the electrochemical stability of the composite. Results have been recently reported based on this strategy. Wu et al. reported the synthesis of chemically modified graphene and PANI nanofiber composites by in situ polymerization of aniline in the presence of graphene oxide; the composites had a high specific capacitance of 480 F/g at a current density 0.1 A/g; and 70% of the original capacitance was retained after 400 cycles in a three-electrode system.[16] Shi et al. prepared composite films of chemically converted graphene and PANI nanofibers by vacuum filtration. The composite films had a specific capacitance of 210 F/g at a current density of 0.3 A/g. The capacitance only decreased 21% after 800 charging−discharging cycles at a current density of 3 A/g.[13] Zhang et al. grew oriented arrays of PANI nanorods on expanded graphite by in situ polymerization, and the composite showed a high specific capacitance of 1665 F/g at a current density of 1 A/g and 87% original capacitance retention after 2000 cycles at a scan rate of 100 mV/s in a three-electrode system.[17] Wang et al. synthesized graphene-wrapped PANI nanofibers with a specific capacitance of 250 F/g at a current density of 0.5 A/g and 74% capacitance retention after 1000 cycles at a current density of 1 A/g in a three-electrode system.[18] Ruoff et al. reported that composites of PANI and graphene oxide afforded a high specific capacitance that could reach 500 F/g at a scan rate of 50 mV s^{-1}, with almost no loss of capacitance over 680 cycles in

Received: April 10, 2013
Accepted: June 21, 2013
Published: June 21, 2013

   dx.doi.org/10.1021/am4013165 | ACS Appl. Mater. Interfaces 2013, 5, 6622−6627

a three-electrode system.[19] However, all of these materials are either relatively complicated to produce, are limited in scalability, or still suffer from the electrochemical stability problem.

In this work, graphene nanoribbons (GNRs), due to their high surface area, high electrical conductivity, and scalability, were selected as a template on which PANI nanorods were grown.[20] A nanocomposite of PANI-GNRs was prepared by the in situ polymerization of aniline in the presence of GNRs. In this composite, GNRs act as the substrate upon which to grow the PANI nanorods, and the GNRs improve the electrical conductivity of the composite, increase the effective utilization of PANI, and enhance the mechanical properties of the composite. The high specific capacitance of the PANI increases the capacitance of the composite. PANI-GNRs displayed good electrochemical properties in energy storage. A specific capacitance of 340 F/g was achieved at a current density of 0.25 A/g in a two-electrode system. The capacity retention was about 90% after 4200 cycles of charging and discharging, making PANI-GNRs a superb electrode material for long-lived energy storage devices.

2. EXPERIMENTAL SECTION

Synthesis of PANI-GNRs. GNRs were prepared by treatment of multiwalled carbon nanotubes (MWCNTs) with NaK in 1,2-dimethoxyethane and quenching of the reaction with MeOH as described previously.[20] The GNRs were then oxidized in 3 M HNO_3 at reflux for 12 h to increase their wettability by introducing hydroxyl functionality and possibly carboxyl groups at the edges. PANI-GNRs were prepared by direct polymerization of aniline on the HNO_3-treated GNRs. In the typical procedure for PANI-GNRs-40, 22.5 mg of HNO_3-treated GNRs was added to 40 mL of 1 M H_2SO_4 solution, and the mixture was ultrasonicated (2510 Branson) to fully disperse the GNRs. Aniline (900 mg, 9.65 mmol) was added to the dispersion, and it was stirred to form a uniform mixture while cooling in a NaCl-ice bath (−3 to −5 °C). The APS oxidant (554 mg, 2.4 mmol), was dissolved in 40 mL of 1 M H_2SO_4 and kept in the NaCl-ice bath for 10 min. The solutions were mixed with continued stirring in the NaCl-ice bath for 10 h. The black solid sample was collected by vacuum filtration and sequentially washing with water (400 mL) and acetone (100 mL). The final PANI-GNRs (130 mg) were obtained after drying in a vacuum oven overnight. In the control experiment, PANI was prepared using the same method above without the HNO_3-treated GNRs. The composite samples were designated as PANI-GNRs-20, -40, or -64 based on the starting weight ratio of aniline to GNRs.

Characterization. Products were characterized by XRD (Rigaku D/Max Ultima II), XPS (PHI Quantera), SEM (JEOL 6500), and TEM (JEM2100F TEM).

Electrochemical Performance Analyses. The electrochemical performance analyses were done using two-electrode system cells with filter paper (Qualitative, Whatman, 1001-042) as a separator between two symmetrical working electrodes. The electrode material was a mixture of 90% active materials and 10% binder polytetrafluoroethylene (PTFE, 60% dispersion in H_2O, Sigma Aldrich). The well-mixed mixture was uniformly pasted on the platinum foil as the current collector. Normally, the average mass per electrode was ∼3.5 mg of active materials and binder. 1 M H_2SO_4 was used as the electrolyte in the performance testing. The prepared two-electrode cell was characterized by CV, galvanostatic charge discharge test, and EIS measurements. An electrochemical station (CHI 660D) was used to perform the above characterization. The gravimetric specific capacitance was obtained from a galvanostatic charge−discharge curve using eq 1[21]

$$C = 4I\Delta t/(\Delta V \times m) \quad (1)$$

where I is the current applied; Δt and ΔV are the discharging time and potential range after the IR drop; and m is the total mass of active materials in two electrodes. The energy density and power density were obtained by using eqs 2 and 3

$$E = CV^2/8 \quad (2)$$

$$P = V^2/(4 \times R \times m) \quad (3)$$

respectively, where C is the specific capacitance; V is the voltage range; m is the total mass of active materials in two electrodes; and R is the equivalent series resistance from the IR drop obtained by eq 4

$$R = V_{drop}/(2I) \quad (4)$$

where V_{drop} is the potential drop at the beginning of the discharge and I is the constant current.

3. RESULTS AND DISCUSSION

The GNRs were prepared through solution-based chemical splitting of carbon nanotubes; the GNRs were edge functionalized with protons by quenching the reaction with MeOH.[20] As shown in Figure S1 (Supporting Information), GNRs were formed that were ∼300 nm wide and several micrometers long. The GNRs were oxidized in 3 M HNO_3 for 12 h at reflux to increase their wettability.[22] The nanocomposites of PANI-GNRs were prepared by the direct polymerization of PANI on GNRs. As depicted in Scheme 1, aniline was adsorbed on GNRs forming active nucleation sites. After the addition of ammonium persulfate (APS), PANI grew outward from the initial nuclei. Ordered, vertically aligned PANI was thus produced on the GNRs. The composite samples were designated as PANI-GNRs-20, -40, or -64 based on the weight ratio of aniline to GNRs: 20:1 (PANI-GNRs-20), 40:1 (PANI-GNRs-40), or 64:1 (PANI-GNRs-64).

Scheme 1. Schematic Illustration of the Synthesis of the PANI-GNR Composite with PANI Polymerized Directly on the GNRs Using APS

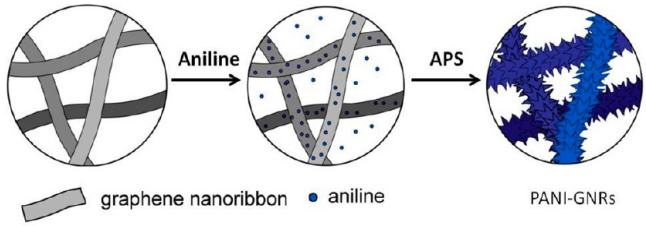

As shown in Figure 1a,b, scanning electron microscopy (SEM) images showed the interesting morphology of the nanocomposite. Figure 1a is a low-resolution SEM image, and Figure 1b is a high-resolution SEM image that shows ordered, vertically aligned PANI directly growing on and around the GNRs, forming one-dimensional wires with porcupine-like quills. The structural detail was also found in the transmission electron microscopy (TEM) images, as shown in Figure 1c,d. TEM images of PANI-GNRs revealed that PANI nanorods covered the external surface of the GNRs. They were ∼20 nm wide and almost 300 nm in length.

X-ray diffraction (XRD) and X-ray photoelectron spectroscopy (XPS) were also used to characterize the nanocomposite PANI-GNRs. Figure 2a shows the XRD pattern of GNRs, pure PANI, and the PANI-GNRs composite. The GNRs showed a strong diffraction peak (002) of graphite at 26.5.[20,23] The XRD pattern of PANI showed three characteristic peaks. The peaks at 2θ of 15.3 and 25.6 resulted from the periodicity both perpendicular and parallel to the polymer chain, respec-

dx.doi.org/10.1021/am4013165 | ACS Appl. Mater. Interfaces 2013, 5, 6622−6627

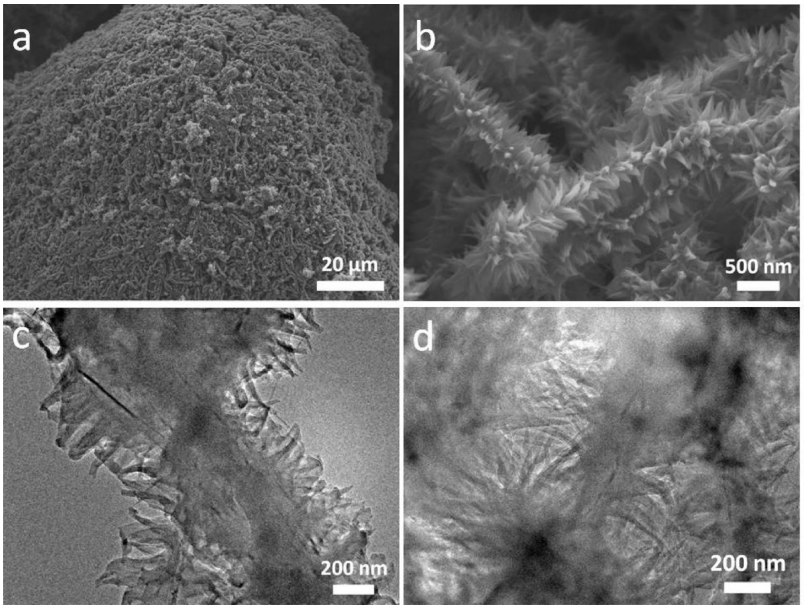

Figure 1. SEM images of composite PANI-GNRs-40 at (a) low resolution and (b) high resolution. (c) and (d) TEM images of composite PANI-GNRs-40.

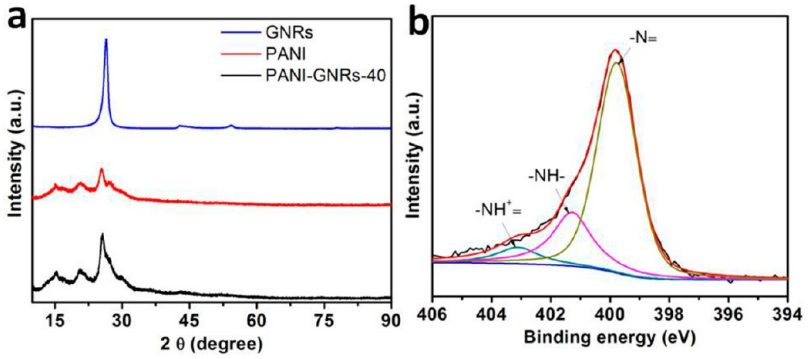

Figure 2. (a) XRD patterns of GNRs, pure PANI, PANI-GNRs-40. (b) N 1s core level X-ray photoelectron spectroscopy (XPS) of PANI-GNRs-40.

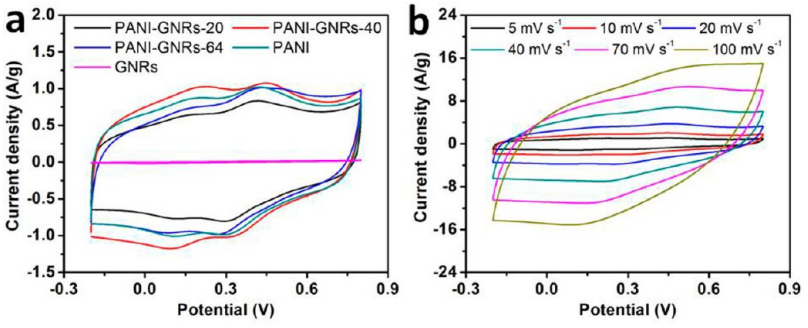

Figure 3. (a) Cyclic voltammetry curves of pure PANI, PANI-GNRs-20, PANI-GNRs-40, and PANI-GNRs-64 at the scan rate of 5 mV s^{-1} in 1 M H_2SO_4. (b) Cyclic voltammetry curves for PANI-GNRs-40 at the scan rate range of 5−100 mV s^{-1} in 1 M H_2SO_4.

tively.[17,24] The peak at 2θ of 21.0 is caused by the layers of polymer chains at alternating distances.[17,25] The XRD pattern of composite PANI-GNRs had similar peaks as PANI, excluding the obvious increase in peak intensity at 26.5 due to the incorporated effect of GNRs in the composite.[17] XPS was used to analyze the composite PANI-GNRs. Figure S2 (Supporting Information) indicates that the composite PANI-GNRs only contained four elements, C, N, O, and trace S from the APS and/or sulfuric acid. As shown in Figure 2b, the deconvolution of the N 1s core-level XPS of PANI-GNRs-40 led to three peaks resulting from three different electronic states: the quinoid amine (−N═) with binding energy centered at 399.74 eV; the benzenoid amine (−NH−) with binding energy centered at 401.28 eV; and the positively charged nitrogen (−NH^+═) with binding energy centered at 403.10 eV.[26−28]

To evaluate the electrochemical performance of PANI-GNRs as active electrode materials, cyclic voltammetry (CV),

dx.doi.org/10.1021/am4013165 | ACS Appl. Mater. Interfaces 2013, 5, 6622−6627

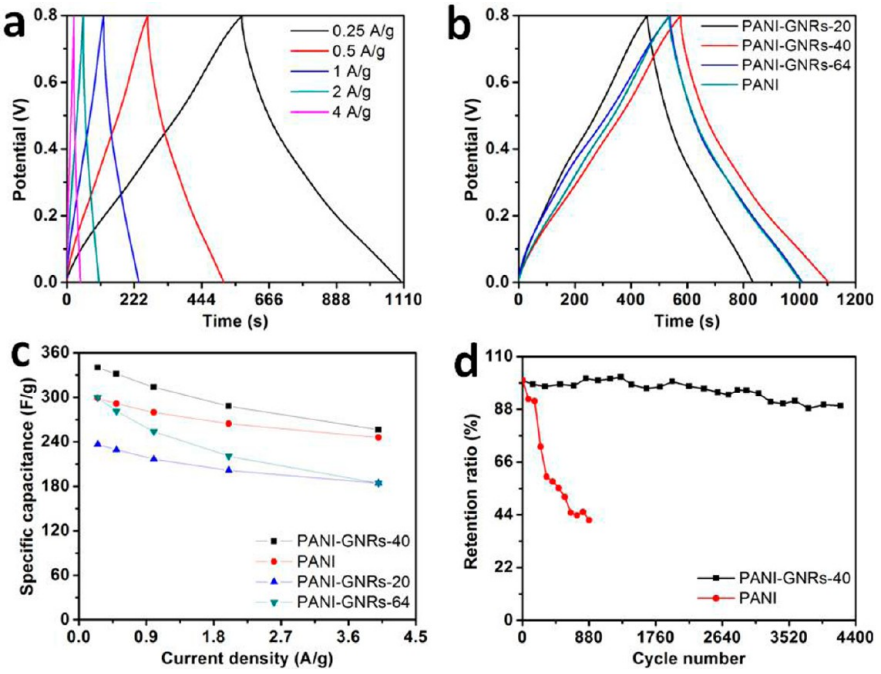

Figure 4. (a) Galvanostatic charge discharge curves of PANI-GNRs-40 at a current density range of 0.25 to 4 A/g. (b) Galvanostatic charge discharge curves of PANI, PANI-GNRs-20, PANI-GNRs-40, and PANI-GNRs-64 at a current density of 0.25 A/g. (c) The specific capacitance versus current density for the pure PANI and composites. (d) Cycling stability of PANI and PANI-GNRs-40 at a current density of 1 A/g.

galvanostatic charge discharge experiments, and electrochemical impedance spectroscopy (EIS) experiments were carried out using a two-electrode configuration in 1 M H_2SO_4 aqueous solution. Figure 3 shows the CV curves of the PANI-GNRs-20, PANI-GNRs-40, PANI-GNRs-64, GNRs, and pure PANI in the potential window range of 0−0.8 V. As shown in Figure3a, the CV curve of GNRs was very small compared to the others, demonstrating that GNRs had almost no contribution to capacitance. On the basis of the data, GNRs improved the electrical conductivity of the composite, and the PANI provided the capacitance. For PANI-GNRs-64, PANI-GNRs-40, PANI-GNRs-20, and pure PANI, there were two pairs of redox peaks in the CV curves at the 5 mV s^{-1} scan rate. The peaks from 0.15 to 0.08 V result from the redox transitions of PANI from leucoemeraldine to emeraldine. The transition in form between emeraldine and pernigraniline leads to the peaks from 0.4 to 0.3 V.[29] Figure 3b shows the CV curves of PANI-GNRs-40 at different scan rates from 5 to 100 mV s^{-1}. The data for pure PANI, PANI-GNRs-20, and PANI-GNRs-64 are shown in Figure S3 (Supporting Information). It is clear that the current response demonstrates a corresponding increase with the scan rate increase. Furthermore, the composite electrode maintained a broad CV shape even at high scan rate up to 100 mV s^{-1}. These characteristics demonstrate a good capacitive behavior of the electrode using the composite materials. Pure PANI and PANI-GNRs-20 had similar characteristics, as shown Figure S3a,b (Supporting Information), while PANI-GNRs-64 was somewhat different at the high scan rate shown in Figure S3c (Supporting Information).

The galvanostatic charge−discharge experiment was also carried out to evaluate the electrochemical properties of the composite. Figure 4a shows the galvanostatic charge−discharge curves of the PANI-GNRs-40 composite in the potential range from 0 to 0.8 V at varying current densities. The almost symmetrical charging and discharging curves demonstrate that the electrode materials had good capacitive behavior. With the increase of the current density, the discharging time gradually reduced. Figure 4b shows the galvanostatic charge−discharge curves of PANI, PANI-GNRs-20, PANI-GNRs-40, and PANI-GNRs-64 at the same current density. On the basis of the galvanostatic charge−discharge curves, the specific capacitance was obtained as shown in Figure 4c. PANI-GNRs-40 produced the best performance. Its specific capacitance was as high as 340 F/g at a current density of 0.25 A/g. With the increase of the current density, the value of specific capacitance decreased to 257 F/g at a current density of 4 A/g. Moreover, the specific capacitance of PANI and PANI-GNRs-20 had similar trends with the variation in current density. At the same current density, the value of specific capacitance of PANI and PANI-GNRs-20 was lower than that of PANI-GNRs-40. The former might result from the low electrical conductivity compared to PANI-GNRs-40 embedded with GNRs, which are presumed to increase the electrical conductivity of the composite. The latter resulted from the high GNR content in the composite, which decreased the value of the specific capacitance. The difference in discharge time of PANI, PANI-GNRs-20, and PANI-GNRs-40 was also consistent with the variation of their CV curves at the same scan rates of 5 mV s^{-1} as shown in Figure 3a. The endurance galvanostatic charge−discharge experiment was also carried out to study the cyclic stability of the composite materials. As shown in Figure 4d, the capacity of PANI decreased quickly: 41% capacity was retained after 880 cycles. Conversely, the capacity retention of PANI-GNRs-40 still remained at ∼90% after 4200 cycles. The large improvement in the cycling performance resulted from the enhanced mechanical resilience of the composite due to the embedded GNRs. Moreover, the special structure of PANI-GNRs-40 is also helpful for the relaxation of the volume expansion during the doping/dedoping process.[1] This demonstrates that the incorporation of GNRs into the composite greatly improves

dx.doi.org/10.1021/am4013165 | ACS Appl. Mater. Interfaces 2013, 5, 6622−6627

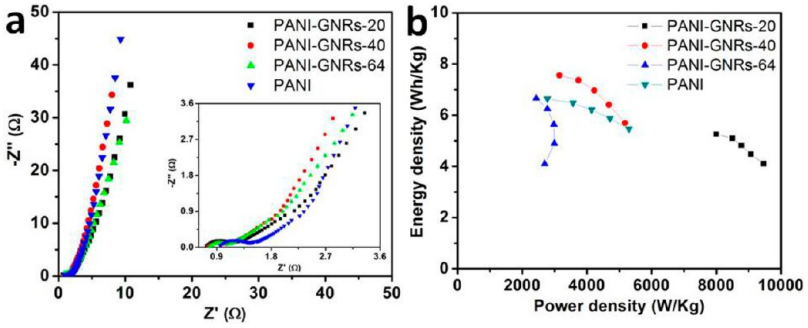

Figure 5. (a) Nyquist plots of PANI, PANI-GNRs-20, PANI-GNRs-40, and PANI-GNRs-64 (the inset is an enlarged view of the Nyquist curves). (b) Ragone plot of PANI, PANI-GNRs-20, PANI-GNRs-40, and PANI-GNRs-64.

the cyclic stability and makes the PANI-GNRs-40 composite a suitable material for energy storage electrodes.

Electrochemical impedance spectroscopy is a powerful tool to study the electrochemical behavior of PANI, PANI-GNRs-20, PANI-GNRs-40, and PANI-GNRs-64 in bulk and at the interface between the electrode and electrolyte.[30−32] The impedance was tested in the frequency range from 20 kHz to 0.01 Hz at the open-circuit potential as shown in Figure 5a. At the higher frequency of 20 kHz, the value of impedance, which is obtained by the intersection between the line and real axes, is the combination of electrolyte resistance and electrode resistance.[33−35] The 45° region in the plots is indicative of the porous structure properties of the PANI-GNRs. At low frequencies, the straight line is nearly perpendicular to the real *y* axis, demonstrating that PANI-GNRs had pure capacitive behaviors.[34,35] The resistance of PANI-GNRs-20 was 0.73 Ω. The value of resistance increased as the GNR content decreased: 0.76 Ω for PANI-GNRs-40, 0.79 Ω for PANI-GNRs-64, and 0.96 Ω for PANI without GNRs. Therefore, more PANI loading in the composite would reduce the conductivity of the electrode. This result was in agreement with the potential variation of the *IR* drop (V_{IR} is 5 mV for PANI-GNRs-20, 12.7 mV for PANI-GNRs-40, 14.4 mV for PANI-GNRs-64, and 15.8 mV for PANI). Figure 5b is the Ragone plot of energy density versus power density for PANI, PANI-GNRs-20, PANI-GNRs-40, and PANI-GNRs-64. PANI-GNRs-40 had the highest energy density of 7.56 Wh/kg with the power density of 3149 W/kg at the current density of 0.25 A/g. PANI-GNRs-20 had the highest power density of 9467 W/kg with an energy density of 4.10 Wh/kg at a current density of 4 A/g. This value was far better than obtained in a conventional supercapacitor.[4,36]

4. CONCLUSION

In summary, ordered, vertically aligned PANI nanorods were grown on GNRs by the direct polymerization of aniline in the presence of GNRs. The nanostructures of the composite PANI-GNRs were characterized by SEM, TEM, XPS, and XRD, and the results indicated that the PANI polymerized on the GNRs. Electrochemical studies demonstrated that synergy between PANI and GNRs affords the composites, showing good electrochemical performance in energy storage, a high specific capacitance, and greatly improved electrochemical stability in the extended time charge discharge process.

■ ASSOCIATED CONTENT

Supporting Information

Additional SEM, XPS, and CV figures. This material is available free of charge via the Internet at http://pubs.acs.org.

■ AUTHOR INFORMATION

Corresponding Author

*E-mail: tour@rice.edu.

Notes

The authors declare no competing financial interest.

■ ACKNOWLEDGMENTS

MI-SWACO/Schlumberger, the Lockheed Martin Corporation through the LANCER IV Program, Sandia National Laboratory, the ONR MURI program (#00006766, N00014-09-1-1066), the Air Force Office of Scientific Research (FA9550-09-1-0581), the AFOSR MURI program (FA9550-12-1-0035), and the Chinese Scholarship Council provided funding for this research.

■ REFERENCES

(1) Zhang, L. L.; Zhao, X. S. *Chem. Soc. Rev.* **2009**, *38*, 2520−2531.
(2) Winter, M.; Brodd, R. J. *Chem. Rev.* **2004**, *104*, 4245−4269.
(3) Miller, J. R.; Simon, P. *Science* **2008**, *321*, 651−652.
(4) Simon, P.; Gogotsi, Y. *Nat. Mater.* **2008**, *7*, 845−854.
(5) Chen, W.; Rakhi, R. B.; Hu, L.; Xie, X.; Cui, Y.; Alshareef, H. N. *Nano Lett.* **2011**, *11*, 5165−5172.
(6) Arico, A. S.; Bruce, P.; Scrosati, B.; Tarascon, J.-M.; van Schalkwijk, W. *Nat. Mater.* **2005**, *4*, 366−377.
(7) Yu, G.; Hu, L.; Vosgueritchian, M.; Wang, H.; Xie, X.; McDonough, J. R.; Cui, X.; Cui, Y.; Bao, Z. *Nano Lett.* **2011**, *11*, 2905−2911.
(8) Xu, J.; Wang, K.; Zu, S.-Z.; Han, B.-H.; Wei, Z. *ACS Nano* **2010**, *4*, 5019−5026.
(9) Feng, X.-M.; Li, R.-M.; Ma, Y.-W.; Chen, R.-F.; Shi, N.-E.; Fan, Q.-L.; Huang, W. *Adv. Funct. Mater.* **2011**, *21*, 2989−2996.
(10) Bhadra, S.; Khastgir, D.; Singha, N. K.; Lee, J. H. *Prog. Polym. Sci.* **2009**, *34*, 783−810.
(11) Wang, Y. G.; Li, H. Q.; Xia, Y. Y. *Adv. Mater.* **2006**, *18*, 2619−2623.
(12) Kang, E. T.; Neoh, K. G.; Tan, K. L. *Prog. Polym. Sci.* **1998**, *23*, 277−324.
(13) Wu, Q.; Xu, Y.; Yao, Z.; Liu, A.; Shi, G. *ACS Nano* **2010**, *4*, 1963−1970.
(14) Li, D.; Huang, J.; Kaner, R. B. *Acc. Chem. Res.* **2008**, *42*, 135−145.
(15) Ryu, K. S.; Kim, K. M.; Park, N.-G.; Park, Y. J.; Chang, S. H. *J. Power Sources* **2002**, *103*, 305−309.
(16) Zhang, K.; Zhang, L. L.; Zhao, X. S.; Wu, J. *Chem. Mater.* **2010**, *22*, 1392−1401.

(17) Li, Y.; Zhao, X.; Yu, P.; Zhang, Q. *Langmuir* **2012**, *29*, 493−500.
(18) Zhou, S.; Zhang, H.; Zhao, Q.; Wang, X.; Li, J.; Wang, F. *Carbon* **2013**, *52*, 440−450.
(19) Lai, L.; Yang, H.; Wang, L.; Teh, B. K.; Zhong, J.; Chou, H.; Chen, L.; Chen, W.; Shen, Z.; Ruoff, R. S.; et al. *ACS Nano* **2012**, *6*, 5941−5951.
(20) Genorio, B.; Lu, W.; Dimiev, A.; Zhu, Y.; Raji, A.-R. O.; Novosel, B.; Alemany, L. B.; Tour, J. M. *ACS Nano* **2012**, *6*, 4231−4240.
(21) Zhao, X.; Zhang, L.; Murali, S.; Stoller, M. D.; Zhang, Q.; Zhu, Y.; Ruoff, R. S. *ACS Nano* **2012**, *6*, 5404−5412.
(22) Bi, R.-R.; Wu, X.-L.; Cao, F.-F.; Jiang, L.-Y.; Guo, Y.-G.; Wan, L.-J. *J. Phys. Chem. C* **2010**, *114*, 2448−2451.
(23) Campos-Delgado, J.; Romo-Herrera, J. M.; Jia, X.; Cullen, D. A.; Muramatsu, H.; Kim, Y. A.; Hayashi, T.; Ren, Z.; Smith, D. J.; Okuno, Y.; et al. *Nano Lett.* **2008**, *8*, 2773−2778.
(24) Pouget, J. P.; Jozefowicz, M. E.; Epstein, A. J.; Tang, X.; MacDiarmid, A. G. *Macromolecules* **1991**, *24*, 779−789.
(25) Li, Y.; Zhao, X.; Xu, Q.; Zhang, Q.; Chen, D. *Langmuir* **2011**, *27*, 6458−6463.
(26) Yue, J.; Epstein, A. J. *Macromolecules* **1991**, *24*, 4441−4445.
(27) An, J.; Liu, J.; Zhou, Y.; Zhao, H.; Ma, Y.; Li, M.; Yu, M.; Li, S. *J. Phys. Chem. C* **2012**, *116*, 19699−19708.
(28) Kim, B.-J.; Oh, S.-G.; Han, M.-G.; Im, S.-S. *Synth. Met.* **2001**, *122*, 297−304.
(29) Li, H.; Wang, J.; Chu, Q.; Wang, Z.; Zhang, F.; Wang, S. *J. Power Sources* **2009**, *190*, 578−586.
(30) Taberna, P. L.; Simon, P.; Fauvarque, J. F. *J. Electrochem. Soc.* **2003**, *150*, A292−A300.
(31) Masarapu, C.; Zeng, H. F.; Hung, K. H.; Wei, B. *ACS Nano* **2009**, *3*, 2199−2206.
(32) Choi, B. G.; Hong, J.; Hong, W. H.; Hammond, P. T.; Park, H. *ACS Nano* **2011**, *5*, 7205−7213.
(33) Hu, L.; Chen, W.; Xie, X.; Liu, N.; Yang, Y.; Wu, H.; Yao, Y.; Pasta, M.; Alshareef, H. N.; Cui, Y. *ACS Nano* **2011**, *5*, 8904−8913.
(34) Sheng, K.; Sun, Y.; Li, C.; Yuan, W.; Shi, G. *Sci. Rep* **2012**, *2*, 247.
(35) Chen, J.; Sheng, K.; Luo, P.; Li, C.; Shi, G. *Adv. Mater.* **2012**, *24*, 4569−4573.
(36) Meng, C.; Liu, C.; Chen, L.; Hu, C.; Fan, S. *Nano Lett.* **2010**, *10*, 4025−4031.